

## RESEARCH ARTICLE

# Self-organized optimal packing of kinesin-5-driven microtubule asters scales with cell size

Neha Khetan<sup>1</sup>, Gérard Pruliere<sup>2</sup>, Celine Hebras<sup>2</sup>, Janet Chenevert<sup>2,\*</sup> and Chaitanya A. Athale<sup>1,\*</sup>

## ABSTRACT

Radial microtubule (MT) arrays or asters determine cell geometry in animal cells. Multiple asters interacting with motors, such as those in syncytia, form intracellular patterns, but the mechanical principles behind this are not clear. Here, we report that oocytes of the marine ascidian *Phallusia mammillata* treated with the drug BI-D1870 spontaneously form cytoplasmic MT asters, or cytasters. These asters form steady state segregation patterns in a shell just under the membrane. Cytaster centers tessellate the oocyte cytoplasm, that is divide it into polygonal structures, dominated by hexagons, in a kinesin-5-dependent manner, while inter-aster MTs form 'mini-spindles'. A computational model of multiple asters interacting with kinesin-5 can reproduce both tessellation patterns and mini-spindles in a manner specific to the number of MTs per aster, MT lengths and kinesin-5 density. Simulations predict that the hexagonal tessellation patterns scale with increasing cell size, when the packing fraction of asters in cells is  $\sim 1.6$ . This self-organized *in vivo* tessellation by cytasters is comparable to the 'circle packing problem', suggesting that there is an intrinsic mechanical pattern-forming module that is potentially relevant to understanding the role of collective mechanics of cytoskeletal elements in embryogenesis.

This article has an associated First Person interview with the first author of the paper.

**KEY WORDS:** Microtubule, Kinesin-5, Aster, Tessellation, Self-organization, Scaling

## INTRODUCTION

Radial arrays of microtubules (MTs) or asters formed from centrosomes or MT-organizing centers (MTOCs) have an intrinsic ability to sense geometry. This has been demonstrated with asters that find the geometric center of a confining compartment based on mechanics alone driven by the balance of radial forces of MT bending and polymerization as seen both *in vitro* (Holy et al., 1997) and in computer simulations (Letort et al., 2016). Similar center-finding by asters *in vitro* has also been demonstrated when dynein motors were anchored at the boundary (Laan et al., 2008, 2012a), recapitulating the role of cortical minus-end-directed molecular motors *in vivo* aster positioning. The importance of the mechanics of aster–motor systems for cell physiology is further emphasized by


evidence for asymmetric force generation resulting in off-center localization of asters driven by polarized distribution of cortical motors during asymmetric cell division as seen in the first embryonic division of *Caenorhabditis elegans* (Colombo et al., 2003; Grill, 2010; Grill and Hyman, 2005; Grill et al., 2001). In larger cells with diameters exceeding 30  $\mu\text{m}$ , where asters do not always contact the cell boundary, intracellular forces originating from cytoplasmic motors, typically dyneins, can drive aster positioning as seen during *C. elegans* fertilization (Kimura and Kimura, 2010; Kimura and Onami, 2005), in *Xenopus* oocyte extracts (Athale et al., 2014) and during sperm aster centering in sea urchin eggs (Tanimoto et al., 2016). Asymmetric forces are then generated either through MT length asymmetry regulated by biochemical gradients (Athale et al., 2008, 2014; Carazo-Salas and Karsenti, 2003; Caudron et al., 2005) or through spatial gradients of motors combined with self-organized clustering (Khetan and Athale, 2016; Schuh and Ellenberg, 2007). More recently, a theoretical model of how pushing and pulling forces drive single aster positioning has been developed and applied to the *C. elegans* embryo (Ma et al., 2014). These studies demonstrate the role of aster–motor mechanics in determining their ability to sense geometry *in vitro*, in intact cells and in simulations.

The role of aster mechanics mediated by motor pushing is prominently seen in *Drosophila melanogaster* embryos, where plus-end-directed motors push apart asters by 'walking' on intercalating astral microtubules (Baker et al., 1993). Such spatial segregation of nuclei into zones of influence were first described as 'energids' in 1892 by J. v. Sachs with reference to syncytia (Mavraklis et al., 2009; Sachs, 1892). The clear separation reported by Sachs in coenocytic algal cells with multiple nuclei is also conserved in animal cells. In more recent work quantifying the ordering of syncytial nuclei in *Drosophila*, nuclei were found to be organized in a hexagonal arrangement driven by astral MTs that persisted even after enucleation, that is, in the absence of nuclear material, suggesting the dominance of cytoskeletal interactions in structure formation (Kanesaki et al., 2011). The forces driving the spacing of the syncytial spindles in *Drosophila* have been shown to be generated by an F-actin network anchoring centrosomal asters *in vivo*, when using embryonic extracts *ex vivo* (Telley et al., 2012) and *in silico* by a mathematical model of the syncytial segregation of nuclei by actin-repulsive forces (Koke et al., 2014). Although the *in vivo* spindle segregation patterns of *Drosophila* syncytium demonstrates the principle of aster–motor segregation patterns, the system involves multiple force generators. It remains unclear whether the collective mechanics of MTs and motors can intrinsically generate the well-separated aster-centered hexagonal structures.

Cytoplasmic MT asters, denoted cytasters, could provide a simpler system to study *in vivo* multi-aster pattern formation. Unfertilized eggs of sea urchin are reported to form cytasters when either the pH of the medium (Kuriyama and Borisy, 1983) or osmolarity (Kallenbach, 1985) is changed, or when MT-stabilizing

<sup>1</sup>Division of Biology, IISER Pune, Dr. Homi Bhabha Road, Pashan, Pune 411008, India. <sup>2</sup>LBDV, Sorbonne Université/CNRS, 06230 Villefranche-sur-Mer, France.

\*Authors for correspondence (chenevert@obs-vlfr.fr; cathale@iiserpune.ac.in)

 N.K., 0000-0001-9972-1921; J.C., 0000-0002-8231-4008; C.A.A., 0000-0002-9506-2153

drugs like paclitaxel are added (Schatten et al., 1982). Indeed varying concentrations of paclitaxel (referred to as taxol) and hexylene glycol have been shown to result in size changes in cytasters as well as the emergence of spirals (Harris and Clason, 1992). Taxol-induced cortical cytasters have also been seen to emerge in mammalian cell lines, in a manner dependent on NuMA1 and minus-end directed kinesin HSET (also known as KifC1) (Hornick et al., 2008). In leech zygotes, taxol treatment results in an orderly movement of cytasters (Cantillana et al., 2000). The primary mechanism driving cytaster formation is thought to be increased MT polymerization either caused by a reduction in the critical concentration of nucleation or by inducing signaling corresponding to the cell cycle (Harris and Clason, 1992). In a recent theoretical model of multi-aster systems in the presence of cortical dynein and cytoplasmic kinesin-5 motors, we find that MT length dynamics and the presence of cortical motors can result in the spontaneous onset of swarming rotational transport (Khetan and Athale, 2020). Our computational model predicts that a minimal system of asters and motors can result in regular aster arrangements, comparable to syncytial systems, requiring nothing other than asters and motors. While such predictions are qualitatively similar to the previously reported patterns, a quantitative comparison to cytasters *in vivo* could reveal a more precise picture of the nature of such self-organization of cytoskeletal elements.

Kinesin-5 in animal cell mitosis walks on MTs originating from pairs of asters at the two poles of a spindle producing stable bipolar structures (Loughlin et al., 2010; Nedelec, 2002) and maintaining spindle length (Yang et al., 2016). However, *in vivo*, both plus-end- and minus-end-directed motors act simultaneously during bipolarization in spindle assembly, as seen in multiple systems such as *Xenopus* oocyte extracts (Boleti et al., 1996; Walczak et al., 1998), *Drosophila* embryos (Sharp et al., 1999) and mammalian cells in culture (Tanenbaum and Medema, 2010). Evidence of the need for antagonistic activity of kinesin-5 and dynein for spindle assembly has accumulated in mammalian cells (Ferenz et al., 2009), and given rise to the principle of a balance of ‘push–pull’ inward and outward forces involving the coordination of three motors – kinesin-5 (Eg5, also known as Kif11), Kif15 and dynein (van Heesbeen et al., 2014). Both dynein and kinesin-5 motors are seen to affect aster migration speeds in developing mouse embryos (Courtois et al., 2012). This suggests that a model which systematically examines the role of antagonistic motor mechanics on multi-aster systems could shed light on cytaster patterns as well as spindle assembly mechanics.

Here, we report kinesin-5-dependent polygonal segregation patterns of MT cytasters in oocytes of the ascidian *Phallusia mammillata* treated with BI-D1870, an inhibitor of the ribosomal S6 kinase (RSK). The pattern quantified by tessellation is comparable to that predicted by a computational model of self-organization of multiple asters with diffusible kinesin-5 motors. We compare model predictions to experiments to determine the role of MT length, kinesin-5 density and motor–aster–MT stoichiometry and use the model to predict the role of a critical packing fraction of asters (i.e. relative area) required for the spontaneous emergence of optimal hexagonal packing of asters.

## RESULTS

### BI-D1870-induced cytasters in *Phallusia* oocytes form a hexagonal lattice

Oocytes of the ascidian *Phallusia mammillata* have increasingly become a model organism to study the role of centrosomal asters in spindle orientation and embryonic division (McDougall et al., 2015). As part of a wider screen of kinase inhibitors for phenotypes in

*Phallusia* cell division and embryogenesis, we tested the effect of the drug BI-D1870 (hereafter referred to as BiD), a dihydropteridinone derivative, that works as a potent ATP-competitive inhibitor of all ribosomal S6 kinase (RSK) isoforms (Bain et al., 2007; Sapkota et al., 2007). RSKs are kinases of the AGC family that regulate multiple processes in somatic cells including translation, proliferation, cell growth and motility (Romeo et al., 2012). Here, we report for the first time that BiD treatment induces the rapid and reproducible formation of multiple cytasters in the peripheral cytoplasm of the *Phallusia* oocyte. These cytasters form a regular network, with each aster consisting of a radial array of MT filaments containing  $\alpha$ -tubulin with a central  $\gamma$ -tubulin localization (Fig. 1A). The MT connections between neighboring asters appear to generate bipolar bundles of MTs resembling mini-spindles (Fig. 1A, lower row). This inhibitor has been routinely used on mammalian cell lines and more recently in mouse oocytes to investigate the function of RSKs in the meiotic cell cycle (Soeda et al., 2018), as well as in neuronal excitability in *Aplysia* (Liu et al., 2020). However, the role of BiD in influencing cytoskeletal dynamics is not well understood, and this effect of cytaster induction has not been reported before. Interestingly, RSK is a component of the MAPK pathway, which is responsible for the suppression of cell cycle progression and MT growth, in eggs of many species (Jesus et al., 2020; McDougall et al., 2012; Stephano and Gould, 2000). Additionally, depletion of

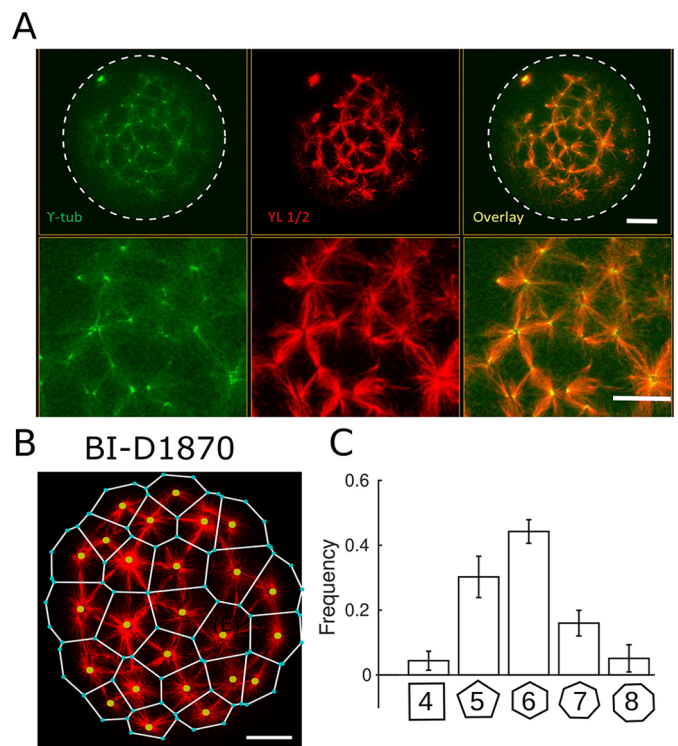


**Fig. 1. BI-D1870-treated *Phallusia* oocytes form multiple cytasters, which tessellate as a hexagonal lattice.** (A) Oocytes of *Phallusia mammillata* treated with 10  $\mu$ M BI-D1870, an RSK inhibitor, were fixed and labeled with antibodies to  $\gamma$ -tubulin (green) and  $\alpha$ -tubulin (red). The overlay image illustrates the  $\gamma$ -tubulin signal is located at the aster centers (yellow). The oocyte perimeter is indicated with the dashed white line. The lower row shows enlarged views. Scale bars: 25  $\mu$ m. (B) Tessellation of a representative *Phallusia* oocyte treated with 10  $\mu$ M BI-D1870 and stained for tubulin (red). Voronoi tessellation of aster centers (yellow circles) resulted in polygon edges (white) and vertices (cyan). Scale bar: 25  $\mu$ m. (C) The frequency distribution of polygon shapes; the numbers of sides (4–8) are indicated along the x-axis. Results represent mean $\pm$ s.d. for 5 oocytes.

RSK in human cells has been seen to result in a loss of MT nucleation and polymerization (Park et al., 2016).

In order to quantify the strikingly regular arrangement of cytasters in the *Phallusia* oocyte, we analyze projected images from confocal z-stacks. We apply Voronoi tessellation from computational geometry, which divides space into convex polygons based on line segments nearest to a pair of neighboring aster centers (Fig. 1B). The resulting lattice consists of cytaster-centered polygons with a range of 4 to 8 sides, predominantly hexagons (Fig. 1C). Qualitatively, this arrangement is analogous to the packing arrangement of atoms in a molecular lattice. We analyzed the cytaster pattern induced by different concentrations of BiD and found that the aster-centered cells tessellate with a predominantly hexagonal geometry (Fig. 2A). We also observed cytaster formation when *Phallusia* oocytes were treated with 10 or 20  $\mu\text{M}$  taxol, a drug known to increase MT nucleation and stabilization, or with 10  $\mu\text{M}$  ammonium chloride, which raises intracellular pH (Fig. 2B). Quantification of the nature of the BiD-induced aster patterns showed that the aster-centered cells tessellate with predominantly hexagonal geometry with increasing concentration, reducing the variability in polygon distribution (Fig. 2C). Taxol- and  $\text{NH}_4\text{Cl}$ -treated aster-centered Voronoi cells also appear to tessellate with hexagons being predominant (Fig. 2D). Increasing BiD concentrations led to a slight increase in the mean number of aster-centered Voronoi ‘cells’, comparable to the number seen in  $\text{NH}_4\text{Cl}$ -treated oocytes, while taxol treatment resulted in a greater number of such ‘cells’ (Fig. 2E). The area per Voronoi cell appears to correspondingly decrease (Fig. 2F), consistent with the well-studied role of taxol in nucleation and stabilization, since more asters spaced out in the same cell would result in smaller polygons. This suggests more nucleation compared to BiD results in shorter

MT lengths, which could be explained by a limiting pool of tubulin. While all three treatments result in cytaster formation, only BiD results in the formation of ‘mini-spindle’ structures.

These results suggest the emergence of arrays of membrane-free compartments as a result of repulsive pushing of MT asters. In order to test whether MT motor mechanical interactions can result in self-organization of the observed structures, we generated a minimal computational model of aster–motor mechanics during confinement within a cell with the aim of determining the conditions for such pattern formation.

### Modeling collective mechanics of multiple aster patterns driven by kinesin-5

We use a computational model to simulate diffusible spring-like discrete motors that act on semi-flexible polymer, which in our case form radial asters. We use an agent-based simulation environment for cytoskeletal mechanics, Cytosim (Nedelec and Foethke, 2007), with parameters of molecular and cellular processes taken either from the literature or specific to *Phallusia* (Tables S1,S2), while simulation parameters were chosen for numerical accuracy (Table S3). The simulated cell is modeled as a rigid circular boundary with radius  $R$  (Fig. 3A). Forces are generated by MTs pushing at the cell boundary generating an inward force,  $F_{\text{MT}}$  (Fig. 3B). The magnitude and direction of the inward force is determined by the degree of curvature, filament length and flexural rigidity ( $\kappa$ ), which is characteristic of the material and based on elastic beam theory, with parameters taken from experimental measurements (Gittes et al., 1993). This model of inward forces generated by MTs pushing at the boundary and bending is consistent with previous reports of confined asters that can spontaneously find the center *in vitro* (Faivre-Moskalenko and

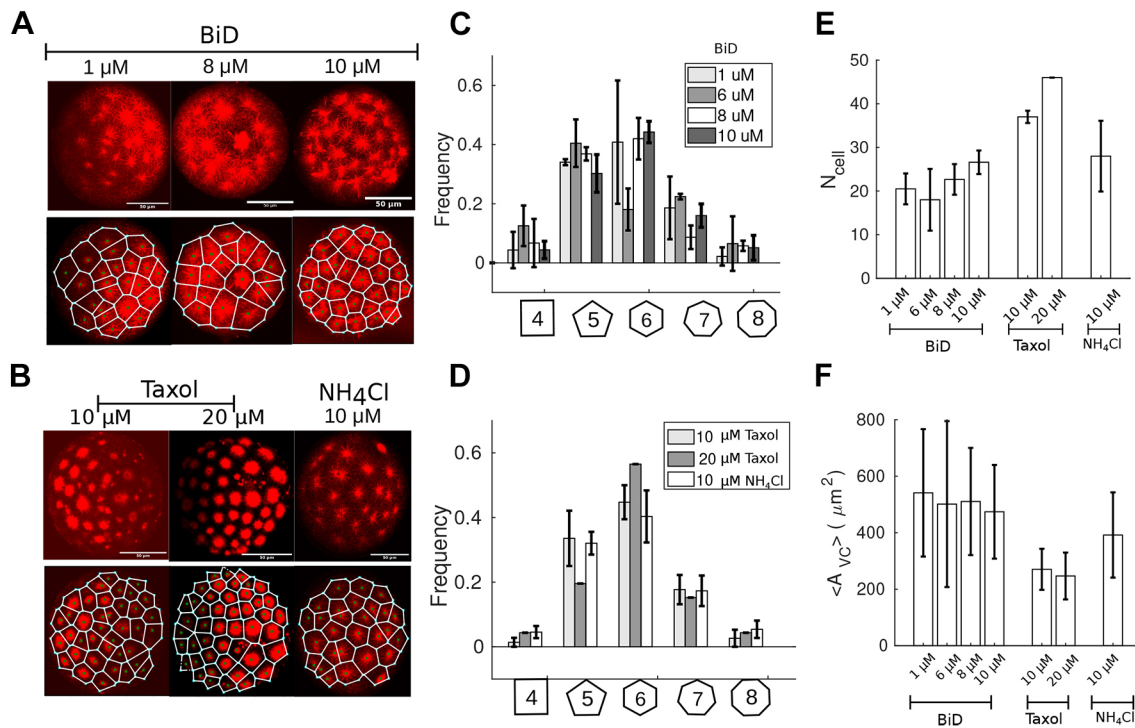


**Fig. 2. Cytaster patterns in *Phallusia* oocytes treated with Bi-D1870, taxol or  $\text{NH}_4\text{Cl}$ .** (A,B) Top rows, representative images of *Phallusia* oocytes treated with the indicated concentrations of (A) BiD (1, 8 or 10  $\mu\text{M}$ ) or (B) Taxol (10 or 20  $\mu\text{M}$ ) or  $\text{NH}_4\text{Cl}$  (10  $\mu\text{M}$ ), fixed and stained with an antibody to  $\alpha$ -tubulin (red). Bottom rows, the same images after Voronoi tessellation. Polygon edges (white lines) separate aster centroids (green circles). Scale bars: 50  $\mu\text{m}$ . (C,D) The polygon distribution of tessellated cytasters in oocytes treated with the indicated range of concentrations of (C) BiD or (D) taxol or  $\text{NH}_4\text{Cl}$ . (E) The number of Voronoi ‘cells’ (polygons) per oocyte ( $N_{\text{cell}}$ ) and (F) the mean area of the Voronoi cell ( $A_{\text{VC}}$ ) are compared across drug treatments. Results are mean $\pm$ s.d. Number of oocytes analyzed ranges between 2 and 8 for each treatment.

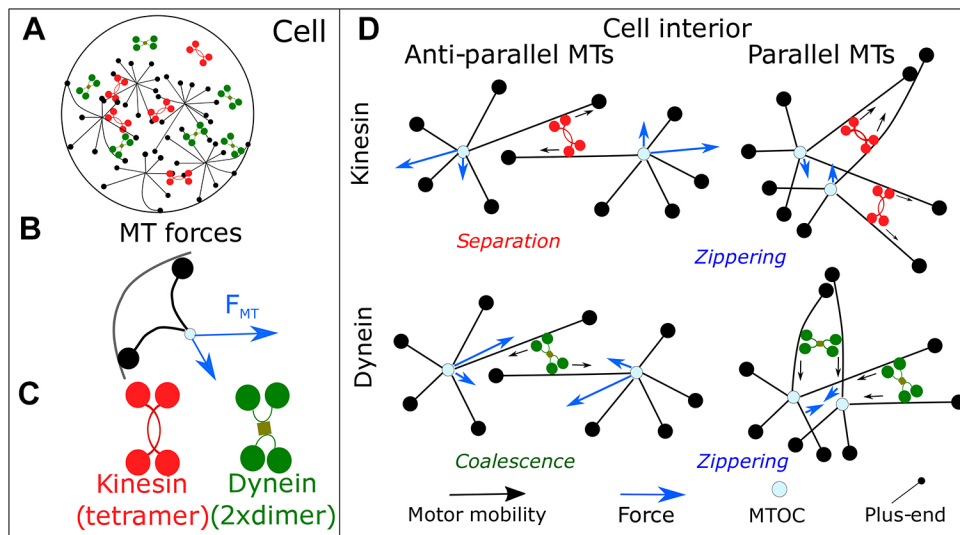


**Fig. 3. Model of multi-aster interactions in a cell.** (A) The minimal 2D model of multiple asters in a circular cell consisting of two kinds of antagonistic motor complexes, kinesin-5 (red) and dynein complexes (green) and microtubules (MT, black lines) arranged as radial arrays or asters with their minus ends embedded in the center and free plus-ends (black circles). (B) Inward forces (blue arrows) act on aster centers (circles) due to a restoring force,  $F_{MT}$ , generated when MTs bend on contact with the rigid cell boundary. (C) The tetrameric kinesin-5 (red) and dynein dimers (green) are modeled as active walking motors with Hookean springs linking the motor heads. (D) The forces acting on asters cross-linked by motors are depicted resulting in either separation, zippering or coalescence of asters, depending on the direction of motor movement (black arrows) and MT orientation. Blue arrows, forces acting on aster centers.

Dogterom, 2002; Holy et al., 1997) in cells (Burakov et al., 2008; Malikov et al., 2005; Zhu et al., 2010) and *in silico* in the geometry of the mouse meiotic oocyte (Khetan and Athale, 2016) or the first embryonic division in *C. elegans* (Ma et al., 2014). We model antagonistic forces due to the activity of kinesin and dynein, plus- and minus-end-directed motors, respectively (Fig. 3C). In the model, we consider the kinesin complexes to be similar to the tetrameric Eg5 motors (Ferenz et al., 2009; Tanenbaum et al., 2008), while dynein complexes are modeled as pair of dimers coupled by a cross-linker, based on previous reports (van Heesbeen et al., 2014). The motor complexes can bind to two different MTs and produce forces on neighboring asters. The nature of forces acting on asters due to motor activity depends on the relative orientation of MTs from a pair of asters and the type of motor complex bound to the MTs: kinesin complexes generate separating forces when walking on anti-parallel MTs, but ‘zipper’ them together when MTs are parallel, while dyneins produce either forces that ‘coalesce’ asters when MTs are anti-parallel or zipper them if MTs are parallel (Fig. 3D). All parameters of single-motor mechanics are based on previous reports with only motor densities varied (Table S2). Since the typical size of asters seen in the *Phallusia* oocytes is  $\sim 10$ -fold smaller than the radius of the cell (Fig. 1B), MT bending-based inward forces are expected to play only a minor role, since asters will rarely contact the cell boundary. In such cases, the effect of the motor complexes will dominate.

In order to determine the simulation geometry, we took recourse to the experimental data. Confocal microscopy *z*-stacks of BiD-treated *Phallusia* oocytes labeled for tubulin demonstrate that cytoplasmic asters are distributed at the cell periphery in 3D forming a ‘shell’ consisting of a lattice of cytasters under the membrane (Fig. 4A; Movie 1). To mimic this distribution, we simulated multiple asters in 3D that were bounded on the outside by a rigid cell membrane, and volume exclusion by an inner mass of the cell center (Fig. 4B). To simplify calculations, we projected the 3D geometry to a 2D circular boundary (Fig. 4B).

Based on previous work, we hypothesized that the activity of the molecular motor kinesin-5 drives the regular arrangement of the cytasters due to repulsive pushing forces seen in spindles (Walczak et al., 1998). In previous reports, such tetrameric kinesins have been shown to separate asters in experiments (Wühr et al., 2009)

and in simulations (Khetan and Athale, 2020). We treated *Phallusia* oocytes first with 50  $\mu\text{M}$  monastrol, an inhibitor of kinesin-5, and then with 10  $\mu\text{M}$  BiD. The resulting tubulin-stained images demonstrated that cytasters were no longer arranged regularly and instead appeared dispersed (Fig. 4C). Over time these structures coalesced into a few, large asters (Fig. S1). In order to test whether the model could reproduce the perturbation of patterns seen in experiments, we simulated multiple asters in the cell with MTs of a fixed length in the presence of a varying kinesin-5 density, from 0 to 1000 motors/ $\mu\text{m}^2$ . We found that the regular segregation patterns depend on the presence of a high density of motors (Fig. 4D). These patterns are steady state as evidenced by simulations of multiple asters with only kinesin-5, only dynein or with no motors (Fig. S2A), which reach a steady state of positions (Fig. S2B) and inter-aster distances (Fig. S2C,D). Increasing the number of MTs per aster did not appear to have a significant effect on the patterns (Fig. S3). MT dynamic instability (i.e. alternating phases of growth and shrinkage of filaments) is known to speed up center finding of asters *in vitro* (Laan et al., 2008). To test the effect on cytaster lattice formation, we varied the flux,  $J$  ( $\mu\text{m/s}$ ), a measure of MT dynamics based on the four-parameter model of dynamic instability (Verde et al., 1992). An increase in MT dynamics was achieved by increasing the magnitude of  $J$  from 0 to  $-0.2785 \mu\text{m/s}$  (Table S4), while maintaining constant mean lengths of MTs ( $L_{MT}$ ). The minus sign of flux indicates bounded growth of MTs, consistent with a steady state mean MT length. The increased flux abrogated the regular patterns observed, even though the kinesin-5 concentration was constant (Fig. 4E). The addition of the antagonistic dynein further reduced the regular patterns in simulations (Figs S4, S5). In these simulations, while dynein and kinesin-5 densities were equal, the mechanical properties of dynein and kinesin were not identical (Table S2). The antagonistic forces do not simply cancel out due to these experimentally reported differences in mechanical properties and the discrete and stochastic nature of the model. This stochastic nature of individual molecules results in a constant motion, binding and unbinding, resulting in fluctuations in net forces.

Thus, we find reduced MT dynamic instability and kinesin-5 are the minimal conditions necessary to produce a stable regular pattern. However, simulations need to be compared to experiments to validate the model predictions.

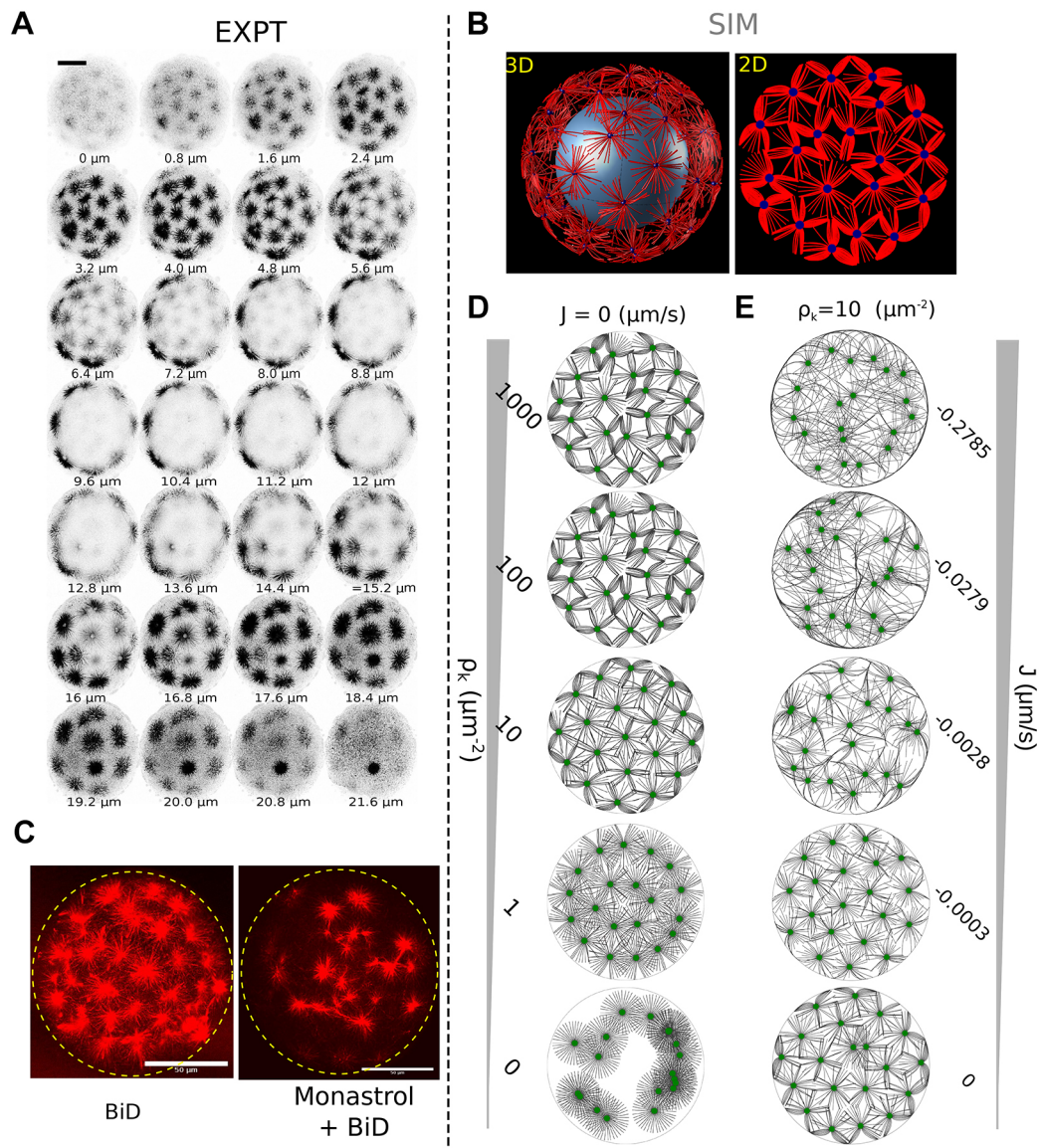


**Fig. 4. 3D distribution of cytasters in oocytes and effect of kinesin-5 in experiment and simulation.** (A) Images from a confocal z-stack of a BiD-treated *Phallusia* oocyte stained for tubulin (inverted grayscale image). The z-position of each image is indicated in  $\mu\text{m}$ . Scale bar: 50  $\mu\text{m}$ . (B) A simulation of multiple asters in 3D with an inner zone (blue sphere) that excludes asters and a rigid outer cell membrane, and the projection in a 2D circular geometry. (C) Tubulin-labeled (red) *Phallusia* oocytes treated with BiD (top) or first treated with monastrol and then BiD (bottom). Scale bars: 25  $\mu\text{m}$ . Dashed circles indicate cell outline. (D) Simulation outputs at steady state depict the effect of decreasing kinesin-5 concentrations (motors/ $\mu\text{m}^2$ ) on multiple asters whose MT lengths are fixed at 4.25  $\mu\text{m}$ . (E) Simulations of the effect of decreasing MT dynamic instability quantified by the flux  $J$  with a constant mean MT length ( $L_{\text{MT}}$  of 4.25  $\mu\text{m}$ ), to test the effect of stochastic MT length fluctuations. The kinesin-5 density ( $\rho_k$ ) is 10 motors/ $\mu\text{m}^2$ . Simulation parameters are common to D and E, and are: cell radius ( $R$ ), 15  $\mu\text{m}$ ; number of asters ( $N_A$ ), 20; and total simulation time, 300 s. EXPT, experimental data from oocytes; SIM, simulations from computational model.

### Simulations predict the spontaneous emergence of ‘mini-spindles’ at high kinesin-5 densities

In simulations, the combination of fixed lengths of MTs, number of cytasters, kinesin-5 motors and a rigid boundary results in the formation of regularly spaced patterns of asters that resemble the striking hexagonal patterns seen in experiments. However, in *Phallusia* oocytes, in addition to the large-scale pattern, we also observed bundled MT arrays that were spindle shaped but lacked chromosomal material at the intersection of three to five asters, which we refer to as ‘mini-spindles’ (Fig. 1A). Such structures are also observed to form spontaneously in simulations at a high kinesin-5 motor density (Fig. 5A). The simulation results imply that

mini-spindles emerge from the mechanical activity of a specific stoichiometry of motors, cytasters, MTs per aster and MT length. In order to test this inference, we compared magnified views of microscopy images from experiments of tubulin-labeled oocytes treated with BiD, taxol and  $\text{NH}_4\text{Cl}$  (Fig. 5B). The absence of such mini-spindles in all conditions except on BiD treatment allows us to hypothesize that the qualitative difference in patterns may result from a ‘depletion effect’. The ratio of the number of motor molecules to number of MT ends long enough to form overlaps would be crucial for mini-spindle formation, and reducing either would lead to either too few ends or too few motors. Assuming the total mass of tubulin is constant, we simulate aster–motor

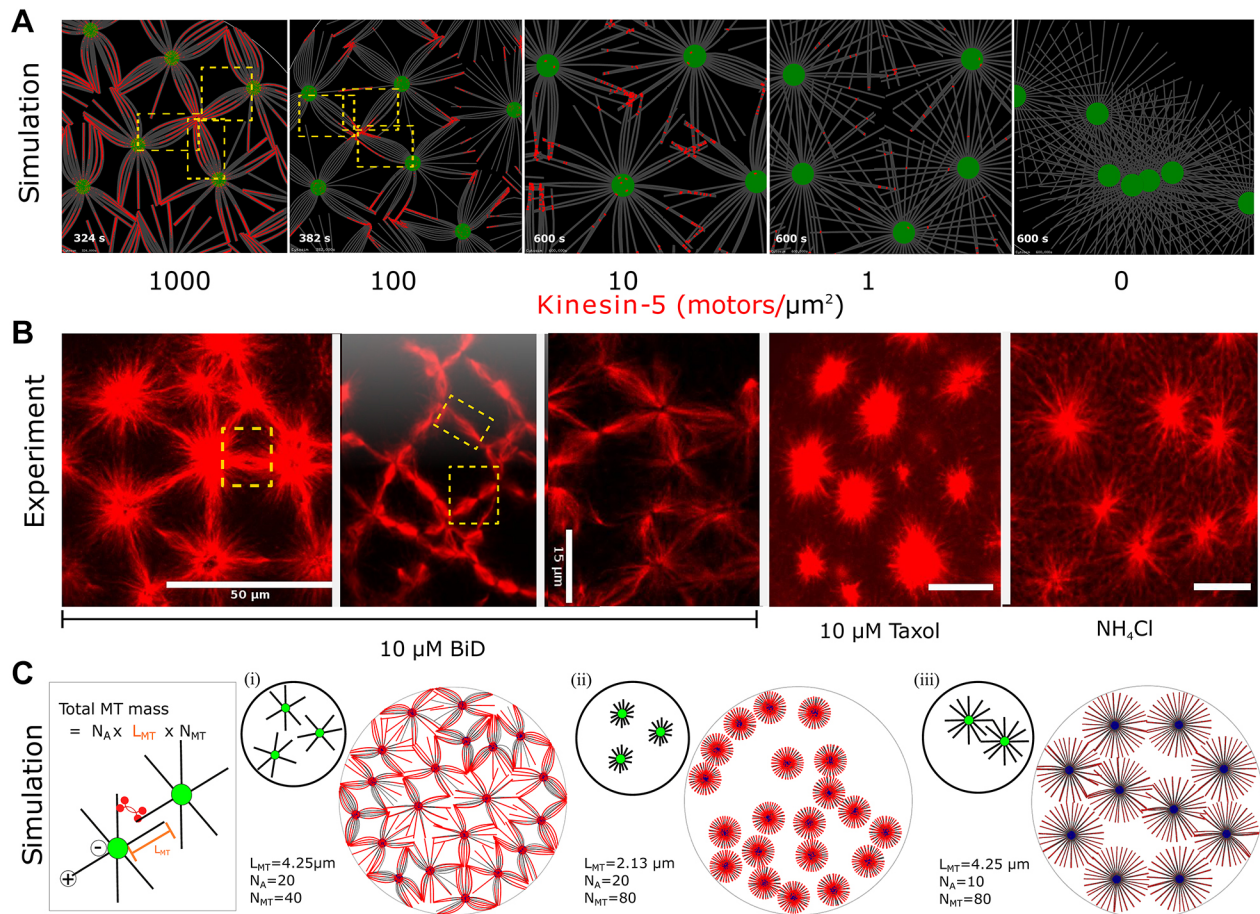


**Fig. 5. Emergence of bipolar 'mini-spindles' in simulation and experiment.** (A) Simulations of multiple asters with increasing density of kinesin-5 ranging from 0 to 1000 motors/ $\mu\text{m}^2$  show the spontaneous formation of mini-spindles (spindle-like but lacking chromatin) highlighted in boxes (yellow). (B) Experimental data from 10  $\mu\text{M}$  BiD-treated oocytes stained for tubulin demonstrate the formation of mini-spindles highlighted with boxes (yellow) that are absent in magnified regions of 10  $\mu\text{M}$  taxol- and 10  $\mu\text{M}$   $\text{NH}_4\text{Cl}$ -treated oocytes. (C) The 'depletion' effect was tested based on a model of constant total MT mass, given by the product of number of asters ( $N_A$ ), MT length ( $L_{MT}$ ) and number of MTs per aster ( $N_{MT}$ ). (i) In simulations comparable to BiD,  $L_{MT}$  was 4.25  $\mu\text{m}$ ,  $N_{MT}$  were 40 and  $N_A$  were 20. Simulations were run with either (ii) MT lengths reduced by 0.5 while the number of MTs/aster was increased 2-fold, (iii) or the number of asters reduced by 0.5, while increasing MTs/aster 2-fold. Kinesin-5 density was kept constant at 100 motors/ $\mu\text{m}^2$ . Insets show a schematic representation of the changing parameters of aster lengths and number.

interaction scenarios, constrained by the conservation relation: MT mass=number of asters $\times$ length of MTs $\times$ number of MTs (Fig. 5C, schematic). To mimic BiD treatment, we simulated the system with parameters of MT lengths of 4.25  $\mu\text{m}$  nucleated by 20 asters with 40 MTs per aster and a kinesin-5 density of 100 motors/ $\mu\text{m}^2$  (Fig. 5Ci). Alternative treatments were mimicked by increasing the number of MTs per aster 2-fold, while reducing MT lengths by one-half, which resulted in a loss of mini-spindle formation (Fig. 5Cii). Conversely, the number of MTs per aster were increased 2-fold while number of asters were reduced by one-half (Fig. 5Ciii). Both of these scenarios resulted in a loss of mini-spindle formation, which indicates that shorter MTs do not form stable interactions after an initial pushing phase, while the increased number of MTs/aster deplete the number of kinesin-5 molecules that can bind each MT. We estimated MT lengths from experimental images of oocytes treated with taxol and  $\text{NH}_4\text{Cl}$  and found their lengths to be shorter than MTs from BiD-treated oocytes (Fig. S6). Additionally, while  $\text{NH}_4\text{Cl}$  treatment appears to result in similar numbers of asters, asters appear to possess fewer and shorter MTs (Fig. 2B,E,F; Fig. S6). Thus, the simulations (Fig. 5C) can predict *in vivo* outcomes, and can be tested in future using more controlled *in vitro* reconstitution experiments.

The utility of an experimentally validated theoretical model is to predict scenarios not seen so far. We therefore proceeded to test whether the model predicts the emergence of hexagonal patterns only at a specific cell and aster size or if the pattern scales with cell size.

#### Predicting scaling of motor-driven aster tessellation patterns with cell size

Our model of multiple aster self-organization by kinesins predicts the emergence of steady-state organized patterns that fill space (Cytosim parameter file available at <https://github.com/athale/cytosimAsterSelfOrg>), which are distinct from the self-organized patterns of vortices, spirals and asters formed by linear MTs interacting with motors (Nédélec et al., 1997, 2001; Surrey et al., 1998). The motor activity appears to result in an effective repulsion of asters to one another, due to MT overlaps, and we can define the specific MT length distribution and motor densities required for agreement with experimental data in BiD-treated *Phallusia* oocytes. The geometric regularity of the patterns suggests a more general underlying property, which is reminiscent of the arrangement of atoms that pack space to a maximal density (Fig. 6A). The general circle packing problem seeks to address the question what

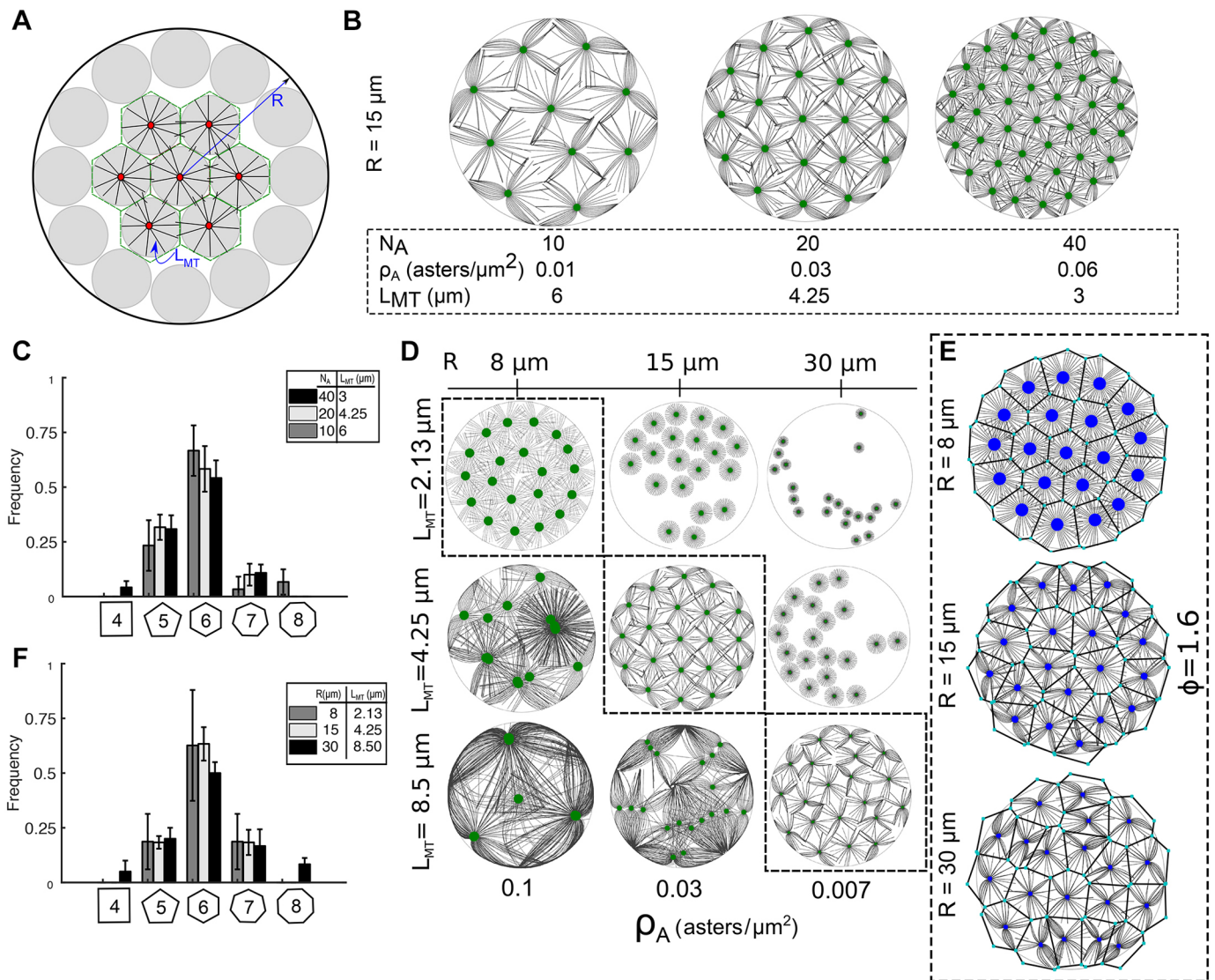


**Fig. 6. Regular patterns of multiple asters depend on packing fraction.** (A) The schematic of patterns formed by asters confined in a larger cell of radius  $R$  with MTs radiating from nucleation centers (red) by MT-overlaps and motor pushing can be understood in terms of polygons (green dashed line) that bound the presumptive circles (gray) with radius corresponding to the length of MTs,  $L_{MT}$ . The packing fraction  $\phi$  is calculated based on the relative area of these average circles and of the circular cell (Eqn 1). (B,C) The packing fraction  $\phi$  of 1.6 results in hexagonal arrangement of asters. We test whether this packing fraction always results in the same patterns, by increasing aster numbers,  $N_A$ , and proportionately decreasing  $L_{MT}$  in a cell of constant size ( $R=15\ \mu\text{m}$ ), and note the resultant (B) steady state aster patterns and (C) polygon frequency distributions in simulations. (D) The steady state aster patterns driven by kinesin are observed when cell radius,  $R$  (x-axis) and aster sizes, i.e.  $L_{MT}$  (y-axis) were independently varied ( $N_A=20$ ). (E,F) The simulation outputs along the diagonal of D that demonstrated regular patterns (dashed boxes) were (E) Voronoi tessellated and (F) their polygon frequency distributions plotted. Total simulation time, 600 s; kinesin density, 10 motors/ $\mu\text{m}^2$ . Aster cores, green circles; MTs, gray lines. In C and F, the numbers of sides (4–8) for the polygon shapes are indicated along the x-axis as mean $\pm$ s.d.

arrangement of uniformly sized circles in two dimensions will maximize the proportion of space covered? The solution attributed to Lagrange (1773) and Gauss (1831) is that 90.69% of the total area is the maximal packing fraction achieved when circles are arranged in a hexagonal lattice defined by their centers (Fejes Tóth, 2017) like a bee's honeycomb. In order to examine whether the aster segregation patterns are related to the general circle packing problem, we quantified the kinesin-driven aster packing density, and tested the hypothesis of whether segregated asters quantitatively follow the rules of optimal packing. Based on this model, we assume the microtubule lengths  $L_{MT}$  are comparable to the radii of circles to be packed, while the cell boundary has a radius  $R$  (Fig. 6A). Kinesin-5 generates the repulsive force between asters by walking to the plus-ends of pairs of MTs from neighboring asters,

analogous to the steric repulsion of circles in the packing problem. We define the packing fraction of asters ( $\phi$ ) as the ratio of the total area of all asters to area of the cell which simplifies to:

$$\phi = \frac{N_A L_{MT}^2}{R^2}. \quad (1)$$

We simulated a constant number and size of multiple asters in a cell whose size was increased and varied the proportion of kinesin-5 and the antagonistic motor dynein. We found that in the absence of antagonistic motors, asters formed a hexagonally packed lattice when  $\phi$  is 1.6 (Fig. S4, Movie 2). The fact that the packing fraction  $\phi$  is greater than one, points to the intercalating nature of the asters, as opposed to the rigid, non-overlapping nature of circles. Such an

overlap is a necessary condition for the observed aster patterns since separating forces between two asters can only be generated when a single kinesin-5 motor can simultaneously bind to two MTs originating from different asters (Fig. 3D). We hypothesize that  $\phi=1.6$  is the optimal aster packing fraction required to generate regular aster arrangements. Consistent with this prediction, we find *Phallusia* oocytes treated with 10  $\mu\text{M}$  BiD have  $\phi=1.3\pm 0.3$  while taxol results in  $\phi=0.48$  and ammonium chloride in  $\phi=0.63$  (Table S5). According to the packing model, the aster pattern should continue to emerge so long as the packing fraction is maintained and motors are not limiting. To test this hypothesis, we simulated the increase in the number of asters,  $N_A$ , while the length of MTs,  $L_{\text{MT}}$ , was proportionately reduced, in order to maintain a constant  $\phi=1.6$  for a cell of constant radius  $R$  (Eqn 1). We found the regular steady state aster patterns were maintained as before for increasing aster density for a constant  $\phi$  both qualitatively (Fig. 6B; Movie 3) and in terms of polygon frequency distribution obtained from tessellation (Fig. 6C). In order to examine scaling of the pattern with cell size and to find physical conditions that abolish these patterns, we varied the cell size  $\sim 2$ -fold, while also varying MT lengths by a similar factor. We fixed the number of asters per cell, as a result of which the aster density varied. We found regular tessellation could be seen only along the diagonal, for which  $\phi$  (Fig. 6D) was to our surprise consistently  $\sim 1.6$  (Fig. 6E,F; Movie 4), and deviations from this packing fraction resulted in a breakdown of order.

We believe these self-organized tessellation patterns arising from steady state aster–motor collective interactions, resemble the geometry of patterns seen in foams of soap bubbles and epithelial tissue sheets, with the major differences that the multi-aster patterns lack a membrane separating the cell-like compartments and require active motor activity for maintenance. Our findings are suggestive of a novel self-organized mechanical intracellular pattern-forming module.

## DISCUSSION

Here, we show that oocytes of *Phallusia mammillata*, a marine ascidian, form multiple microtubule asters when treated with BI-D1870. These cytasters self-organize to form regular tessellation patterns with a predominantly hexagonal geometry. We find the cytaster patterns are the result of collective mechanics of MT asters and kinesin-5 motors based on disruption of this organization by monastrol, an inhibitor of kinesin-5 activity. In order to better understand the patterns, we developed a minimal model of kinesin-5 and multiple asters with only local interactions. We found that increasing kinesin-5 activity results in the spontaneous emergence of a regularly spaced lattice of asters in simulation, reproducing the hexagonal geometry. The model also demonstrates the formation of ‘mini-spindle’ structures that lack chromosomes at high kinesin-5 densities. These structures depend on the stoichiometry of MT lengths, numbers and motor density. The model predicts that MT nucleation and elongation play a vital role, consistent with the difference in cytaster patterns we see between oocytes treated with BiD compared to those treated with taxol and ammonium chloride. We test the generality of the model predictions by examining whether patterns are specific to a particular aster density, cell size or MT length. One property that stands out as a predictor of the ability of these asters to form regular structures is the area packing fraction  $\phi$ . We observe consistent hexagonal patterns when  $\phi$  is  $\sim 1.6$ . We treat this as a special case of the general ‘circle packing’ problem, with intercalation. Consistent with the packing analogy, the patterns scale with cell size when the optimal packing fraction is maintained.

While self-organized pattern formation by linear MT filaments and motors has been widely reported (Nédélec et al., 1997, 2001; Surrey et al., 1998), the ability of more than two asters to self-organize had so far not been quantified in experiments. Previously, it has been shown that asters transported by either plus- or minus-end directed immobilized motors (i.e. a gliding assay), experience a tug of war due to their inherent radial geometry (Athale et al., 2014; Khetan and Athale, 2016). Reports of a kinesin gliding assay with antiparallel MT doublets (comparable to a ‘1D aster’) demonstrated that a similar tug-of-war arising from geometry could be resolved through length asymmetry (Leduc et al., 2010). Experiments that demonstrated how single asters find the geometric center of artificial cells without any signaling, through MT bending mechanics and length dynamics (Faivre-Moskalenko and Dogterom, 2002; Holy et al., 1997) in combination with cortical force generators like dynein (Laan et al., 2012b), have improved our general understanding of the role of mechanics in aster spatial patterns and their dependence on cell size. While MT pushing forces may dominate in small cells, the positioning of asters in large cells is driven by combinations of multiple mechanisms, such as the activity of immobilized motors (Wühr et al., 2009), gradients of MT regulators resulting in asymmetric pulling forces (Athale et al., 2008; Carazo-Salas and Karsenti, 2003; Caudron et al., 2005), diffusible dyneins that cluster asters (Schuh and Ellenberg, 2007), dynein-like motors localized on intracellular organelles (Kimura and Kimura, 2010) and diffusible kinesins that separate astral MTs (Ferenz et al., 2009; Waitzman and Rice, 2014). At the same time MT pushing by astral MTs at the cell boundary appears to play a vital role *in vivo*, as seen in male pronuclear aster centration in sea urchin zygotes (Meaders and Burgess, 2020; Meaders et al., 2020). Therefore, a comprehensive picture that reconciles data across model organisms can be best achieved by modeling the mechanics of aster positioning and potential constraints specific to each system, if we are in future to understand the general principles governing the process.

The model we describe in this study is based on the self-organizing ability of multi-aster systems to form patterns without assuming any spatial heterogeneity or guidance cues. The model is based on local interactions – coupling by molecular motors and the mechanics of MT pushing at the cell boundary. By simplifying the geometry of the system based on a projection into a plane of the 3D system, we find the model can explain the structures seen in large cells of *Phallusia* oocytes. Our model could be relevant for understanding spindle alignment and spacing in syncytial systems, such as the *Drosophila* embryo, in which aster spacing patterns show a similar dependence on MT length in combination with the role of actin (Telley et al., 2012), as well as other embryos with meroblastic cleavage patterns such as those of fish, spider, locust or the sea anemone (Tamulonis et al., 2011). Indeed, a wide variety of reproductive strategies involve multiple asters sharing the same cytoplasm, including physiological polyspermy, parthenogenesis and cases of naturally occurring cytasters that might be capable of forming such patterns. In future, a more complex model that invokes spindle mechanics, and the role of the acto-myosin network, could be used to address the diversity of alignment patterns seen in these syncytial systems.

The regularity of tessellations seen in nature, in foams of soap bubbles, decorative tiling patterns and molecular arrangements, points to universal laws underlying such patterns (Thompson, 1917). The self-organized emergence of a tiling pattern in aster–motor interactions is novel but not unexpected as demonstrated in our previous theoretical study of the role of cortical dynein and



stochasticity in driving self-organized aster rotation (Khetan and Athale, 2020). At a multi-cellular scale, the properties of membrane adhesion and mechanics have been shown to explain the statistics of polygon formation based on soap bubble foam theory in the case of *Drosophila* epithelial tissue (Farhadifar et al., 2007) and plant meristematic tissue (Corson et al., 2009). However, the structures we report here emerge in the absence of membrane enclosures, by the pushing of asters by kinesin-5 and the boundary effect of the cell membrane. The scaling predictions of our simulations can be potentially tested by reconstitution approaches, such as those where linear MT filaments and motors encapsulated in lipid monolayer droplets have been seen to self-organize (Baumann and Surrey, 2015) as well as *Xenopus* oocyte extracts that self-organize into membrane-free compartments driven by MTs and dynein motors, independently of centrosomal asters and chromosomes (Cheng and Ferrell, 2019). While it remains unclear whether such self-organized intracellular sub-compartments have any functional role to play, the intrinsic ability of MT–motor mechanics to generate subcellular compartments provides an opportunity to apply a synthetic cell biology approach to better understand principles of cellular organization (Mitchison and Field, 2019). In that sense, we believe our results suggest chemically treated *Phallusia* oocytes could potentially serve as an alternative model to *Xenopus* extracts.

Thus, in our study we have quantified the kinesin-5-dependent cytaster patterns induced by BiD treatment in oocytes of *Phallusia* using tessellation, and find the predominance of hexagons. We have developed a mechanically detailed model of radial MT arrays or asters interacting with motors, and show that a minimal model of kinesin-5 and asters can produce similar tessellation structures by self-organization of local interactions. The model prediction of the emergence of mini-spindles dependent on aster number, MT lengths and kinesin-5 density is tested by comparison with taxol treatment. The aster tessellation pattern emerges only for a specific packing density which scales with cell size as well as with aster size and density. We believe these results point to a novel *in vivo* mechanical pattern-forming system, which could be relevant for understanding the emergence of membrane-free compartmentalization.

## MATERIALS AND METHODS

### Computer simulations of collective aster–motor mechanics

#### Model geometry

The cell was modeled as a 2D circular space with a confined boundary. MTs, on contacting the cortex, experienced an inward force. The cortex was modeled as a spring. The restoring force was calculated using Hooke's law where  $k_c$ , the spring constant, determined the stiffness of confinement (Corson et al., 2009).

#### MT and aster mechanics

MTs were simulated as flexible rods with a flexural rigidity ( $\kappa$ ) based on previous experimental reports (Letort et al., 2016). The lengths of MTs were either kept constant (static) or varied (dynamic) during the simulation. In those calculations where MTs were dynamic, length changes of MTs were modeled based on the two-state four-parameter model (Dogterom and Leibler, 1993), and the parameters were based on the estimates from *ex vivo* studies in *Xenopus* oocytes (Verde et al., 1992). The flux of MTs was measured using the expression  $J = (v_g * f_r - v_s * f_c) / (f_c + f_r)$ , where  $f_c$  and  $f_r$  are the frequencies of rescue and catastrophe, while  $v_g$  and  $v_s$  are the velocities of growth and shrinkage, respectively. The aster was modeled as a radial array of MT filaments nucleating isotropically from a central point. For visualization, a central circle represented the aster center. At initialization, asters were distributed in the cell based on a random uniform density. Aster positions were updated based on the net forces experienced due to the combination of MT dynamics, forces experienced by the MTs at the cortex

and the MT–motor interactions (Athale et al., 2008; Carazo-Salas and Karsenti, 2003).

#### Motor model

Inspired from experiments, motor complexes that can bind to two MT filaments at the same time and couple them, such as tetramers of kinesin (kinesin-5) and coupled dimers of dynein, were modeled as tetrameric motors. A pair of dimeric motors is joined by a Hookean-like component with the stiffness determined by the spring constant,  $k_m$ . A complex can stochastically attach to MTs at a rate  $r_a$ , if it is within the range of the binding distance  $d_a$ . Once a motor dimeric head binds to an MT, the other dimeric part of the complex can bind to MTs in the neighborhood with the same rate  $r_a$ , if it is within a distance  $d_a$ , independently of the orientation of the second MT with respect to the first, that is, whether the MTs are parallel or anti-parallel. Each complex can walk on the MT with a speed ( $v$ ) which is linearly dependent on the load force ( $f$ ) experienced by the complex (Khetan and Athale, 2016) as described by the following equation:

$$v = v_0 \left( 1 - \frac{f}{f_s} \right), \quad (2)$$

where  $v_0$  is the single molecule load free velocity of the motor and  $f_s$  is the stall force threshold. The bound complex can detach stochastically with a detachment rate  $r_d$  that increases exponentially with the load force  $f$  acting on the motor:

$$r_d = r_0 e^{f/f_a}, \quad (3)$$

where  $r_0$  is the single molecule unbinding rate of motor under no load,  $f$  is the magnitude of the load force experienced by the motor and  $f_a$  corresponds to the single molecule unbinding force threshold of the motor. While we model kinesin detachment from the MT to be instantaneous when it reaches the plus-end (Korneev et al., 2007; Loughlin et al., 2010), the unbinding rate of dynein is determined by  $r_d$ , uniformly along the length of the MT.

#### Simulations

All simulations were performed in 2D using Cytosim, a C++-based simulation engine based on Langevin dynamics (Nedelec and Foethke, 2007) where motor–MT interactions are affected by the thermal energy,  $k_B T$  of  $4.2 \times 10^{-21}$  Nm. A typical simulation was run for a total time ( $t$ ) of 600 s. A typical run with number of asters ( $N_A$ ) of 20, MT lengths ( $L_{MT}$ ) of 4.25  $\mu\text{m}$  and  $7 \times 10^3$  kinesin complexes required  $\sim 7$  h to run on a 12-processor (Intel Xeon E5 2630) workstation with 15.6 GB RAM.

#### Animal and oocyte collection

Adults of the ascidian *Phallusia mammillata* were collected in the Etang de Tau (Mediterranean coast, France) and maintained in aquaria with running seawater for a maximum of 4 months. Oocytes were collected by dissection and dechorionated using trypsin protease as described previously (McDougall et al., 2012, 2015). After dechorionation, washed oocytes were stored in gelatin-coated Petri dishes at 18°C for up to 8 h.

#### Pharmacological treatments

All chemical inhibitors were prepared as 1000 $\times$  stock solutions in DMSO. Stock solutions were: BI-D1870, 10 mM (RSKII inhibitor, Calbiochem, CAS 501437-28-1, Merck KGaA, Germany); monastrol, 50 mM (mitotic kinesin EG-5 inhibitor, Calbiochem, CAS 254753-54-3, Merck KGaA, Germany); and taxol, 20 mM (Paclitaxel, Sigma-Aldrich, Merck KGaA, Germany). Treatment with BI-D1870 inhibitor was carried out by incubating oocytes in sea water supplemented with the drug at the desired concentration for 1 hour at 18°C. For double-inhibitor experiments, *Phallusia* eggs were incubated in monastrol (final concentration 50  $\mu\text{M}$ ) for 30 min prior to addition of BI-D1870 (final concentration 10  $\mu\text{M}$ ) and then subject to further incubation for 60–120 min.  $\text{NH}_4\text{Cl}$  (Sigma-Aldrich) was prepared as a 10 mM stock solution in distilled water.

## Immunostaining and microscopy

The primary antibodies used were: anti- $\alpha$  tubulin mouse monoclonal DM1A antibody (cat. no. T9026, 1:1000 dilution), anti-tyrosinated  $\alpha$  tubulin rat monoclonal YL1/2 (cat. no. MAB1864, 1:1000 dilution) and anti- $\gamma$  tubulin mouse monoclonal GTU88 antibody (cat. no. T5326, 1:200 dilution), all from Sigma-Aldrich, Merck KGaA, Germany. Staining oocytes for aster visualization with either DM1A or YL1/2 gave similar results. Secondary anti-mouse or anti-rat-IgG antibodies coupled to fluorescein isothiocyanate (FITC) or to tetramethylrhodamine (TMR) isothiocyanate (Jackson ImmunoResearch Laboratories, West Grove, PA, USA) were used at a dilution of 1:200. For fixation, inhibitor treated or control (DMSO-treated) *Phallusia* eggs were plunged rapidly into cold ( $-20^{\circ}\text{C}$ ) methanol containing 50 mM EGTA, pH 7.5. For immunolabeling, fixed samples were rehydrated via three 5-min washes in phosphate-buffered saline (PBS) and blocked by three 15-min washes in PBT [PBS, pH 7.4, containing 3% bovine serum albumin (BSA) and 0.05% Triton X-100], before incubation with primary antibodies (diluted in PBT) for either 2 h at room temperature or overnight at  $4^{\circ}\text{C}$ . Eggs were then washed three times in PBT, incubated with secondary antibodies supplemented with 1  $\mu\text{g}/\text{ml}$  Hoechst 33342 (Sigma-Aldrich) to label DNA, washed again in PBT, and mounted on glass slides in antifading reagent Citifluor (Chem Lab, Canterbury, UK). Fluorescence images of fixed immunolabeled samples were acquired as z-stacks ( $<2\ \mu\text{m}$  step size) using a  $40\times$  oil objective on a Leica SP5 confocal microscope (Leica Microsystems GmbH, Wetzlar, Germany).

## Image and data analysis

Images of *Phallusia* oocytes were cropped to include the cell boundary visible from the background-level staining of tubulin using ImageJ (Schneider et al., 2012). Maximum projections of the top or bottom portions of each confocal z-stack were made separately and used for tessellation. Polygon analysis from experimental and simulation data was performed using an in-house developed Python (ver. 3.0) script based on the function *voronoi* in the spatial package of SciPy (<https://www.scipy.org/>; Virtanen et al., 2020). Aster centroids from simulations or experiments were provided as inputs to the code and the algorithm identifies the tessellated cells and outputs the polygon statistics including sidedness, area and nearest neighbor distance (NND). All plots were generated using MATLAB R2017b (Mathworks Inc., MA, USA). In order to estimate MT lengths from individual cytasters, we developed a script in MATLAB R2017b based on a previously described method, where the user interactively selects the aster center and the outermost limit of the individual aster to generate a radial intensity profile that is fitted to an exponential distribution to obtain the decay length (Fig. S6).

The code for the aster–motor simulations is available on GitHub at <https://github.com/nedelec/cytosim> and the parameter file ‘phallusia\_fig4d.cym’ (to generate outputs seen in Fig. 4D), is accessible on GitHub at <https://github.com/athale/cytosimAsterSelfOrg>. The custom-made Python script used for Voronoi tessellation is available on request from the corresponding author (C.A.A.).

## Acknowledgements

We thank Alex McDougall for reagents and discussions. We are grateful to Deepak Dhar for pointing out the connection of our work to the general circle packing problem, and Girish Deshpande for critically reading the manuscript. For care and maintenance of animals, we thank the Service Aquariologie of the Institut de la Mer de Villefranche (IMEV), supported by EMBR-CE France.

## Competing interests

The authors declare no competing or financial interests.

## Funding

The work was in part supported by a grant from the Department of Biotechnology, Ministry of Science and Technology, India (BT/PR6715/GBD/27/463/2012) and travel support by the Indo-French Centre for the Promotion of Advanced Research (CEFIPRA) (IFC/0036/2017/1222) to C.A.A. N.K. was supported by a fellowship from the Council for Scientific and Industrial Research [09/936(0128)/2015-EMR-1], the Department of Biotechnology, Ministry of Science and Technology, India (BT/PR6715/GBD/27/463/2012) and CEFIPRA (IFC/0036/2017/1222).

## Author contributions

Conceptualization: J.C., C.A.A.; Methodology: N.K., G.P., C.H., J.C.; Software: N.K.; Validation: N.K., J.C., C.A.A.; Formal analysis: C.A.A.; Investigation: N.K., G.P., C.H., J.C., C.A.A.; Resources: J.C., C.A.A.; Data curation: J.C.; Writing - original draft: J.C., C.A.A.; Writing - review & editing: J.C., C.A.A.; Visualization: G.P., J.C., C.A.A.; Supervision: J.C., C.A.A.; Project administration: C.A.A.; Funding acquisition: C.A.A.

## Peer review history

The peer review history is available online at <https://journals.biologists.com/jcs/article-lookup/doi/10.1242/jcs.257543>

## References

- Athale, C. A., Dinarina, A., Mora-Coral, M., Pugieux, C., Nedelec, F. and Karsenti, E. (2008). Regulation of microtubule dynamics by reaction cascades around chromosomes. *Science* **322**, 1243–1247. doi:10.1126/science.1161820
- Athale, C. A., Dinarina, A., Nedelec, F. and Karsenti, E. (2014). Collective behavior of minus-ended motors in mitotic microtubule asters gliding toward DNA. *Phys. Biol.* **11**, 16008. doi:10.1088/1478-3975/11/11/016008
- Bain, J., Plater, L., Elliott, M., Shpiro, N., Hastie, C. J., Mclauchlan, H., Klevernic, I., Arthur, J. S. C., Alessi, D. R. and Cohen, P. (2007). The selectivity of protein kinase inhibitors: a further update. *Biochem. J.* **408**, 297–315. doi:10.1042/BJ20070797
- Baker, J., Theurkauf, W. E. and Schubiger, G. (1993). Dynamic changes in microtubule configuration correlate with nuclear migration in the preblastoderm *Drosophila* embryo. *J. Cell Biol.* **122**, 113–121. doi:10.1083/jcb.122.1.113
- Baumann, H. and Surrey, T. (2015). Self-organization of motors and microtubules in lipid-monolayered droplets. *Methods Cell Biol.* **128**, 39–55. doi:10.1016/bs.mcb.2015.01.015
- Boleti, H., Karsenti, E. and Vernos, I. (1996). Xklp2, a novel *Xenopus* centrosomal kinesin-like protein required for centrosome separation during mitosis. *Cell* **84**, 49–59. doi:10.1016/S0092-8674(00)80992-7
- Burakov, A., Kovalenko, O., Semenova, I., Zhapparova, O., Nadezhkina, E. and Rodionov, V. (2008). Cytoplasmic dynein is involved in the retention of microtubules at the centrosome in interphase cells. *Traffic* **9**, 472–480. doi:10.1111/j.1600-0854.2007.00698.x
- Cantillana, V., Urrutia, M., Ubilla, A. and Fernandez, J. (2000). The complex dynamic network of microtubule and microfilament cytasters of the leech zygote. *Dev. Biol.* **228**, 136–149. doi:10.1006/dbio.2000.9931
- Carazo-Salas, R. E. and Karsenti, E. (2003). Long-range communication between chromatin and microtubules in *Xenopus* egg extracts. *Curr. Biol.* **13**, 1728–1733. doi:10.1016/j.cub.2003.09.006
- Caudron, M., Bunt, G., Bastiaens, P. and Karsenti, E. (2005). Spatial coordination of spindle assembly by chromosome-mediated signaling gradients. *Science* **309**, 1373–1376. doi:10.1126/science.1115964
- Cheng, X. and Ferrell, J. E. (2019). Spontaneous emergence of cell-like organization in *Xenopus* egg extracts. *Science* **366**, 631–637. doi:10.1126/science.aav7793
- Colombo, K., Grill, S. W., Kimple, R. J., Willard, F. S., Siderovski, D. P. and Gönczy, P. (2003). Translation of polarity cues into asymmetric spindle positioning in *Caenorhabditis elegans* embryos. *Science* **300**, 1957–1961. doi:10.1126/science.1084146
- Corson, F., Hamant, O., Bohn, S., Traas, J., Boudaoud, A. and Couder, Y. (2009). Turning a plant tissue into a living cell froth through isotropic growth. *Proc. Natl. Acad. Sci. USA* **106**, 8453–8458. doi:10.1073/pnas.0812493106
- Courtois, A., Schuh, M., Ellenberg, J. and Hiragi, T. (2012). The transition from meiotic to mitotic spindle assembly is gradual during early mammalian development. *J. Cell Biol.* **198**, 357–370. doi:10.1083/jcb.201202135
- Dogterom, M. and Leibler, S. (1993). Physical aspects of the growth and regulation of microtubule structures. *Phys. Rev. Lett.* **70**, 1347–1350. doi:10.1103/PhysRevLett.70.1347
- Faivre-Moskalenko, C. and Dogterom, M. (2002). Dynamics of microtubule asters in microfabricated chambers: the role of catastrophes. *Proc. Nat. Acad. Sci. USA* **99**, 16788–16793. doi:10.1073/pnas.252407099
- Farhadifar, R., Röper, J.-C., Aigouy, B., Eaton, S. and Jülicher, F. (2007). The influence of cell mechanics, cell-cell interactions, and proliferation on epithelial packing. *Curr. Biol.* **17**, 2095–2104. doi:10.1016/j.cub.2007.11.049
- Fejes Tóth, G. (2017). Packing and covering. In *Handbook of Discrete and Computational Geometry*, 3rd edn (ed. C. D. Toth, J. O'Rourke and J. E. Goodman), pp. 27–93. Boca Raton: Chapman & Hall/CRC. doi:10.1201/9781315119601
- Ferenz, N. P., Paul, R., Fagerstrom, C., Mogilner, A. and Wadsworth, P. (2009). Dynein antagonizes EG5 by crosslinking and sliding antiparallel microtubules. *Curr. Biol.* **19**, 1833–1838. doi:10.1016/j.cub.2009.09.025
- Gauss, C. F. (1831). Untersuchungen über die Eigenschaften der positiven ternären quadratischen Formen von Ludwig August Seeber, *Göttingische gelehrte Anzeigen*. Reprinted in: *Werke (1863)*, Vol. 2, pp. 188–196. Göttingen: Königliche Gesellschaft der Wissenschaften; *J. Reine Angew. Math.* **20**, 312–320.

- Gittes, F., Mickey, B., Nettleton, J. and Howard, J. (1993). Flexural rigidity of microtubules and actin filaments measured from thermal fluctuations in shape. *J. Cell Biol.* **120**, 923-934. doi:10.1083/jcb.120.4.923
- Grill, S. W. (2010). Cell biology, forced to be unequal. *Science* **330**, 597-598.
- Grill, S. W. and Hyman, A. A. (2005). Spindle positioning by cortical pulling forces. *Dev. Cell* **8**, 461-465. doi:10.1016/j.devcel.2005.03.014
- Grill, S. W., Gönczy, P., Stelzer, E. H. and Hyman, A. A. (2001). Polarity controls forces governing asymmetric spindle positioning in the *Caenorhabditis elegans* embryo. *Nature* **409**, 630-633. doi:10.1038/35054572
- Harris, P. J. and Clason, E. L. (1992). Conditions for assembly of tubulin-based structures in unfertilized sea urchin eggs. Spirals, monasters and cytasters. *J. Cell. Sci.* **102**, 557-567.
- Holy, T. E., Dogterom, M., Yurke, B. and Leibler, S. (1997). Assembly and positioning of microtubule asters in microfabricated chambers. *Proc. Natl. Acad. Sci. USA* **94**, 6228-6231. doi:10.1073/pnas.94.12.6228
- Hornick, J. E., Bader, J. R., Tribble, E. K., Trimble, K., Breunig, J. S., Halpin, E. S., Vaughan, K. T. and Hinchcliffe, E. H. (2008). Live-cell analysis of mitotic spindle formation in taxol-treated cells. *Cell Motil. Cytoskeleton* **65**, 595-613. doi:10.1002/cm.20283
- Jessus, C., Munro, C. and Houlston, E. (2020). Managing the oocyte meiotic arrest-lessons from frogs and jellyfish. *Cells* **9**, 1150. doi:10.3390/cells9051150
- Kallenbach, R. J. (1985). Ultrastructural analysis of the initiation and development of cytasters in sea-urchin eggs. *J. Cell. Sci.* **73**, 261-278.
- Kanesaki, T., Edwards, C. M., Schwarz, U. S. and Grosshans, J. (2011). Dynamic ordering of nuclei in syncytial embryos: a quantitative analysis of the role of cytoskeletal networks. *Integr. Biol.* **3**, 1112-1119. doi:10.1039/c1ib00059d
- Khetan, N. and Athale, C. A. (2016). A motor-gradient and clustering model of the centripetal motility of MTOCs in meiosis I of mouse oocytes. *PLoS Comput. Biol.* **12**, e1005102. doi:10.1371/journal.pcbi.1005102
- Khetan, N. and Athale, C. A. (2020). Aster swarming by symmetry breaking of cortical dynein transport and coupling kinesins. *Soft Mat.* **16**, 8554-8564. doi:10.1039/D0SM01086C
- Kimura, K. and Kimura, A. (2010). Intracellular organelles mediate cytoplasmic pulling force for centrosome centration in the *Caenorhabditis elegans* early embryo. *Proc. Nat. Acad. Sci. USA* **108**, 137-142. doi:10.1073/pnas.1013275108
- Kimura, A. and Onami, S. (2005). Computer simulations and image processing reveal length-dependent pulling force as the primary mechanism for *C. elegans* male pronuclear migration. *Dev. Cell* **8**, 765-775. doi:10.1016/j.devcel.2005.03.007
- Koke, C., Kanesaki, T., Grosshans, J., Schwarz, U. S. and Dunlop, C. M. (2014). A computational model of nuclear self-organisation in syncytial embryos. *J. Theor. Biol.* **359**, 92-100. doi:10.1016/j.jtbi.2014.06.001
- Korneev, M. J., Lakämper, S. and Schmidt, C. F. (2007). Load-dependent release limits the processive stepping of the tetrameric Eg5 motor. *Eur. Biophys. J.* **36**, 675-681. doi:10.1007/s00249-007-0134-6
- Kuriyama, R. and Borisy, G. G. (1983). Cytasters induced within unfertilized sea-urchin eggs. *J. Cell. Sci.* **61**, 175-189.
- Laan, L., Husson, J., Munteanu, E. L., Kerssemakers, J. W. J. and Dogterom, M. (2008). Force-generation and dynamic instability of microtubule bundles. *Proc. Natl. Acad. Sci. U.S.A.* **105**, 8920-8925. doi:10.1073/pnas.0710311105
- Laan, L., Pavin, N., Husson, J., Romet-Lemonne, G., van Duijn, M., López, M. P., Vale, R. D., Jülicher, F., Reck-Peterson, S. L. and Dogterom, M. (2012a). Cortical dynein controls microtubule dynamics to generate pulling forces that position microtubule asters. *Cell* **148**, 502-514. doi:10.1016/j.cell.2012.01.007
- Laan, L., Roth, S. and Dogterom, M. (2012b). End-on microtubule-dynein interactions and pulling-based positioning of microtubule organizing centers. *Cell Cycle* **11**, 3750-3757. doi:10.4161/cc.21753
- Lagrange, J. C. (1773). Recherches d'arithmétique. In *Nouv. Mém. Acad. Roy. Belles Lettres Berlin*, 265-312: *Œuvres complète (1869)*, Vol. 3, pp. 693-758. Paris: Gauthier-Villars.
- Leduc, C., Pavin, N., Jülicher, F., Diez, S., Jülicher, F. and Diez, S. (2010). Collective behavior of antagonistically acting kinesin-1 motors. *Phys. Rev. Lett.* **105**, 1-4. doi:10.1103/PhysRevLett.105.128103
- Letort, G., Nedelec, F., Blanchoin, L. and Théry, M. (2016). Centrosome centering and decentering by microtubule network rearrangement. *Mol. Biol. Cell* **27**, 2833-2843. doi:10.1091/mbc.e16-06-0395
- Liu, R.-Y., Zhang, Y., Smolen, P., Cleary, L. J. and Byrne, J. H. (2020). Role of p90 ribosomal S6 kinase in long-term synaptic facilitation and enhanced neuronal excitability. *Sci. Rep.* **10**, 608. doi:10.1038/s41598-020-57484-y
- Loughlin, R., Heald, R. and Nédélec, F. (2010). A computational model predicts *Xenopus* meiotic spindle organization. *J. Cell Biol.* **191**, 1239-1249. doi:10.1083/jcb.201006076
- Ma, R., Laan, L., Dogterom, M., Pavin, N. and Jülicher, F. (2014). General theory for the mechanics of confined microtubule asters. *New J. Phys.* **16**, 13018. doi:10.1088/1367-2630/16/1/013018
- Malikov, V., Cyttrynbaum, E. N., Kashina, A., Mogilner, A. and Rodionov, V. (2005). Centering of a radial microtubule array by translocation along microtubules spontaneously nucleated in the cytoplasm. *Nat. Cell Biol.* **7**, 1113-1118. doi:10.1038/ncb1332
- Mavrakis, M., Rikhy, R. and Lippincott-Schwartz, J. (2009). Cells within a cell: Insights into cellular architecture and polarization from the organization of the early fly embryo. *Commun. Integr. Biol.* **2**, 313-314. doi:10.4161/cib.2.4.8240
- McDougall, A., Chenevert, J. and Dumollard, R. (2012). Cell-cycle control in oocytes and during early embryonic cleavage cycles in ascidians. *Int. Rev. Cell Mol. Biol.* **297**, 235-264. doi:10.1016/B978-0-12-394308-8.00006-6
- McDougall, A., Chenevert, J., Pruliere, G., Costache, V., Hebras, C., Salez, G. and Dumollard, R. (2015). Centrosomes and spindles in ascidian embryos and eggs. *Methods Cell Biol.* **129**, 317-339. doi:10.1016/bs.mcb.2015.03.006
- Meaders, J. L. and Burgess, D. R. (2020). Microtubule-based mechanisms of pronuclear positioning. *Cells* **9**, 505. doi:10.3390/cells9020505
- Meaders, J. L., de Matos, S. N. and Burgess, D. R. (2020). A pushing mechanism for microtubule aster positioning in a large cell type. *Cell Rep.* **33**, 108213. doi:10.1016/j.celrep.2020.108213
- Mitchison, T. J. and Field, C. M. (2019). Toward synthetic cells. *Science* **366**, 569-570. doi:10.1126/science.aaz5635
- Nédélec, F. (2002). Computer simulations reveal motor properties generating stable antiparallel microtubule interactions. *J. Cell Biol.* **158**, 1005-1015. doi:10.1083/jcb.200202051
- Nedelec, F. and Foethke, D. (2007). Collective Langevin dynamics of flexible cytoskeletal fibers. *New J. Phys.* **9**, 427.
- Nédélec, F. J., Surrey, T., Maggs, A. C. and Leibler, S. (1997). Self-organization of microtubules and motors. *Nature* **389**, 305-308. doi:10.1038/38532
- Nédélec, F., Surrey, T. and Maggs, A. C. (2001). Dynamic concentration of motors in microtubule arrays. *Phys. Rev. Lett.* **86**, 3192-3195. doi:10.1103/PhysRevLett.86.3192
- Park, Y. Y., Nam, H.-J., Do, M. and Lee, J.-H. (2016). The p90 ribosomal S6 kinase 2 specifically affects mitotic progression by regulating the basal level, distribution and stability of mitotic spindles. *Exp. Mol. Med.* **48**, e250-e250. doi:10.1038/emmm.2016.61
- Romeo, Y., Zhang, X. and Roux, P. P. (2012). Regulation and function of the RSK family of protein kinases. *Biochem. J.* **441**, 553-569. doi:10.1042/BJ20110289
- Sachs, J. (1892). Physiologische notizen, II. Beiträge zur zelltheorie. energiden und zellen. *Flora* **75**, 57-67.
- Sapkota, G. P., Cummings, L., Newell, F. S., Armstrong, C., Bain, J., Frodin, M., Grauert, M., Hoffmann, M., Schnapp, G., Steegmaier, M. et al. (2007). Bi-D1870 is a specific inhibitor of the p90 RSK (ribosomal S6 kinase) isoforms in vitro and in vivo. *Biochem. J.* **401**, 29-38. doi:10.1042/BJ20061088
- Schatten, G., Schatten, H., Bestor, T. H. and Balczon, R. (1982). Taxol inhibits the nuclear movements during fertilization and induces asters in unfertilized sea urchin eggs. *J. Cell Biol.* **94**, 455-465. doi:10.1083/jcb.94.2.455
- Schneider, C. A., Rasband, W. S. and Eliceiri, K. W. (2012). NIH Image to ImageJ: 25 years of image analysis. *Nat. Methods* **9**, 671-675. doi:10.1038/nmeth.2089
- Schuh, M. and Ellenberg, J. (2007). Self-organization of MTOCs replaces centrosome function during acentrosomal spindle assembly in live mouse oocytes. *Cell* **130**, 484-498. doi:10.1016/j.cell.2007.06.025
- Sharp, D. J., Yu, K. R., Sisson, J. C., Sullivan, W. and Scholey, J. M. (1999). Antagonistic microtubule-sliding motors position mitotic centrosomes in *Drosophila* early embryos. *Nat. Cell Biol.* **1**, 51-54. doi:10.1038/9025
- Soeda, S., Yamada-Nomoto, K., Michiue, T. and Ohsugi, M. (2018). RSK-MASTL pathway delays meiotic exit in mouse zygotes to ensure paternal chromosome stability. *Dev. Cell* **47**, 363-376.e5. doi:10.1016/j.devcel.2018.09.011
- Stephano, J. L. and Gould, M. C. (2000). MAP kinase, a universal suppressor of sperm centrosomes during meiosis?. *Dev. Biol.* **222**, 420-428. doi:10.1006/dbio.2000.9726
- Surrey, T., Elowitz, M. B., Wolf, P.-E., Yang, F., Nédélec, F., Shokat, K. and Leibler, S. (1998). Chromophore-assisted light inactivation and self-organization of microtubules and motors. *Proc. Natl. Acad. Sci. USA* **95**, 4293-4298. doi:10.1073/pnas.95.8.4293
- Tamulonis, C., Postma, M., Marlow, H. Q., Magie, C. R., de Jong, J. and Kaandorp, J. (2011). A cell-based model of *Nematostella vectensis* gastrulation including bottle cell formation, invagination and zippering. *Dev. Biol.* **351**, 217-228. doi:10.1016/j.ydbio.2010.10.017
- Tanenbaum, M. E. and Medema, R. H. (2010). Mechanisms of centrosome separation and bipolar spindle assembly. *Dev. Cell* **19**, 797-806. doi:10.1016/j.devcel.2010.11.011
- Tanenbaum, M. E., Macůrek, L., Galjart, N. and Medema, R. H. (2008). Dynein, Lis1 and CLIP-170 counteract Eg5-dependent centrosome separation during bipolar spindle assembly. *EMBO J.* **27**, 3235-3245. doi:10.1038/emboj.2008.242
- Tanimoto, H., Kimura, A. and Minc, N. (2016). Shape-motion relationships of centering microtubule asters. *J. Cell Biol.* **212**, 777-787. doi:10.1083/jcb.201510064
- Telley, I. A., Gáspár, I., Ephrussi, A. and Surrey, T. (2012). Aster migration determines the length scale of nuclear separation in the *Drosophila* syncytial embryo. *J. Cell Biol.* **197**, 887-895. doi:10.1083/jcb.201204019
- Thompson, D. A. W. (1917). On growth and form. *Nature* **100**, 21-22.
- van Heesbeen, R. G., Tanenbaum, M. E. and Medema, R. H. (2014). Balanced activity of three mitotic motors is required for bipolar spindle assembly and

- chromosome segregation. *Cell Rep.* **8**, 948-956. doi:10.1016/j.celrep.2014.07.015
- Verde, F., Dogterom, M., Stelzer, E., Karsenti, E. and Leibler, S.** (1992). Control of microtubule dynamics and length by cyclin A- and cyclin B-dependent kinases in *Xenopus* egg extracts. *J. Cell Biol.* **118**, 1097-1108. doi:10.1083/jcb.118.5.1097
- Virtanen, P., Gommers, R., Oliphant, T. E., Haberland, M., Reddy, T., Cournapeau, D., Burovski, E., Peterson, P., Weckesser, W., Bright, J. et al.** (2020). SciPy 1.0: fundamental algorithms for scientific computing in Python. *Nat. Methods* **17**, 261-272. doi:10.1038/s41592-019-0686-2
- Waizman, J. S. and Rice, S. E.** (2014). Mechanism and regulation of kinesin-5, an essential motor for the mitotic spindle. *Biol. Cell* **106**, 1-12. doi:10.1111/boc.201300054
- Walczak, C. E., Vernos, I., Mitchison, T. J., Karsenti, E. and Heald, R.** (1998). A model for the proposed roles of different microtubule-based motor proteins in establishing spindle bipolarity. *Curr. Biol.* **8**, 903-913. doi:10.1016/S0960-9822(07)00370-3
- Wühr, M., Dumont, S., Groen, A. C., Needleman, D. J. and Mitchison, T. J.** (2009). How does a millimeter-sized cell find its center? *Cell Cycle* **8**, 1115-1121. doi:10.4161/cc.8.8.8150
- Yang, C. F., Tsai, W. Y., Chen, W. A., Liang, K. W., Pan, C. J., Lai, P. L., Yang, P. C. and Huang, H. C.** (2016). Kinesin-5 contributes to spindle-length scaling in the evolution of cancer toward metastasis. *Sci. Rep.* **6**, 1-9. <https://doi.org/10.1038/srep35767>
- Zhu, J., Burakov, A., Rodionov, V. and Mogilner, A.** (2010). Finding the cell center by a balance of dynein and myosin pulling and microtubule pushing: a computational study. *Mol. Biol. Cell* **21**, 4418-4427. doi:10.1091/mbc.e10-07-0627